HHS Public Access

Author manuscript

Hum Brain Mapp. Author manuscript; available in PMC 2016 March 08.

Published in final edited form as:

Hum Brain Mapp. 2015 May ; 36(5): 1908–1924. doi:10.1002/hbm.22745.

Determination of the Posterior Boundary of Wernicke's Area Based on Multimodal Connectivity Profiles

Jiaojian Wang[1,†], **Lingzhong Fan**[2,3,†], **Yinyan Wang**[4,†], **Wenting Xu**[1], **Tao Jiang**[4], **Peter T. Fox**[5], **Simon B. Eickhoff**[6,7], **Chunshui Yu**[8], and **Tianzi Jiang**[1,2,3,9,*]

[1]Key Laboratory for NeuroInformation of the Ministry of Education, School of Life Science and Technology, University of Electronic Science and Technology of China, Chengdu, China

[2]Brainnetome Center, Institute of Automation, Chinese Academy of Sciences, Beijing, China

[3]National Laboratory of Pattern Recognition, Institute of Automation, Chinese Academy of Sciences, Beijing, China

[4]Beijing Neurosurgical Institute, Capital Medical University, Beijing, China

[5]Research Imaging Institute, University of Texas Health Science Center at San Antonio, Texas

[6]Institute of Neuroscience and Medicine (INM-1), Research Centre Julich, Germany

[7]Institute of Clinical Neuroscience and Medical Psychology, Heinrich Heine University, Dusseldorf, Germany

[8]Department of Radiology, Tianjin Medical University General Hospital, Tianjin, China

[9]The Queensland Brain Institute, University of Queensland, Brisbane, QLD, Australia

Abstract

Wernicke's area is one of the most important language regions and has been widely studied in both basic research and clinical neurology. However, its exact anatomy has been controversial. In this study, we proposed to address the anatomy of Wernicke's area by investigating different connectivity profiles. First, the posterior superior temporal gyrus (STG), traditionally called "Wernicke's area", was parcellated into three component subregions with diffusion MRI. Then, whole-brain anatomical connectivity, resting-state functional connectivity (RSFC) and meta-analytic connectivity modeling (MACM) analyses were used to establish the anatomical, resting-state and task-related coactivation network of each subregion to identify which subregions participated in the language network. In addition, behavioral domain analysis, meta-analyses of semantics, execution speech, and phonology and intraoperative electrical stimulation were used to determine which subregions were involved in language processing. Anatomical connectivity, RSFC and MACM analyses consistently identified that the two anterior subregions in the posterior STG primarily participated in the language network, whereas the most posterior subregion in the temporoparietal junction area primarily participated in the default mode network. Moreover, the behavioral domain analyses, meta-analyses of semantics, execution speech and phonology and

[*]Correspondence to: Tianzi Jiang; Brainnetome Center, Institute of Automation, Chinese Academy of Sciences, Beijing 100190, China. jiangtz@nlpr.ia.ac.cn.

[†]These authors equally contributed to this work.

intraoperative electrical stimulation mapping also confirmed that only the two anterior subregions were involved in language processing, whereas the most posterior subregion primarily participated in social cognition. Our findings revealed a convergent posterior anatomical border for Wernicke's area and indicated that the brain's functional subregions can be identified on the basis of its specific structural and functional connectivity patterns.

Keywords

parcellation; anatomical connectivity; resting-state; meta-analytic connectivity modeling; behavioral domain analysis; intraoperative electrical stimulation

INTRODUCTION

Wernicke's area, which is one of the most classical language regions, remains a useful concept in both basic research and clinical settings [Binder et al., 2000; Geschwind, 1970; Mason et al., 2014; Price et al., 2011; Ross, 2010; Sarubbo et al., 2012; Tomasi and Volkow, 2012]. However, compared with Broca's area, the exact function and anatomy of Wernicke's area has been controversial [Bogen and Bogen, 1976; Brodmann, 1909; DeWitt and Rauschecker, 2013; Geschwind, 1972; Mesulam, 1998; Rauschecker and Scott, 2009a; Shalom and Poeppel, 2008]. Wernicke's area has traditionally been defined as the posterior superior temporal gyrus (STG) and accepted as playing a pivotal role in word comprehension [Ross, 2010]. Later, the left posterior superior temporal sulcus [Price, 2000], the angular gyrus, the supramarginal gyrus (SMG), and the middle temporal gyrus (MTG) were also defined as parts of Wernicke's area [Bogen and Bogen, 1976; Rauschecker and Scott, 2009a]. Furthermore, functional diversity of Wernicke's area, including speech perception and production [Buchsbaum et al., 2001; Hickok and Poeppel, 2000], decoding discourse semantics [Tanner, 2007], auditory word-form recognition and inner speech [DeWitt and Rauschecker, 2013], has been reported in different studies. In the absence of a clear definition of the function and anatomy of Wernicke's area, we may be missing a portion of the brain that is significant in auditory language processing [Musiek et al., 2011].

To delineate the exact location of Wernicke's area, many efforts have utilized task-based neuroimaging [Abrams et al., 2013; Blank et al., 2002; Wise et al., 2001] and lesion-based mapping techniques [Boatman et al., 2000b; Sarubbo et al., 2012]. However, because of the limitations of these two techniques [Bates et al., 2003; Ross, 2010], task-based neuroimaging approach and lesion-based mapping technique can only identify the rough anatomical location which may be involved in a specific function. Thus, the exact location of Wernicke's area is still unresolved. Therefore, a new avenue for addressing this problem is needed. In this paper, we propose to determine the location of Wernicke's area by parcellating this area into functional subregions based on its anatomical connectivity patterns, which can inform the segregation of functionally distinct areas by defining the information it receives and the influence it exerts on other brain areas [Averbeck et al., 2009; Passingham et al., 2002]. That anatomical boundaries can be identified by connectivity profiles has been supported by many studies [Behrens et al., 2003a; Cohen et al., 2009; Fan et al., 2014; Johansen-Berg et al., 2004; Li et al., 2013; Liu et al., 2013;

Neubert et al., 2014; Sallet et al., 2013; Thiebaut de Schotten et al., 2014; Wang et al., 2012, 2015; Zhang et al., 2014]. With diffusion magnetic resonance imaging, we could trace the large fiber tracts in the living human brain to obtain the pattern of anatomical connectivity of Wernicke's area. Thus, the anatomical boundaries of functional subregions of Wernicke's area will be able to be determined based on distinct anatomical connectivity patterns.

Our goal in this paper was to determine the posterior boundary of Wernicke's area and confirm the possible functions of Wernicke's area using multimodal imaging techniques. Our method is based on the following criteria: if a subregion of the brain belongs to Wernicke's area, it should be involved in the language network and participate in language processing. We first delineated a liberal mask in the posterior temporal gyrus, including the areas previously reported to be part of Wernicke's area, and parcellated this area into subregions. Then, we mapped the whole-brain anatomical connectivity, whole brain resting-state and task-dependent coactivation [Laird et al., 2009b] functional network to identify which subregions participated in the language network. In addition, behavioral domain analyses, meta-analyses of semantics, execution speech, phonology and intraoperative electrical stimulation mapping were performed to further confirm which subregions were involved in language processing.

MATERIALS AND METHODS

Participants

Three sets of diffusion-weighted data were used to investigate the subdivision of the posterior STG by cross-validating the parcellation results from the various databases. Dataset 1 was in-house data. Datasets 2 and 3 were accessed from community-shared samples (NKI/Rockland sample and Beijing: Eyes Open Eyes Closed Study, web link: http://fcon_1000.projects.nitrc.org/). For Dataset 1, 10 healthy, right-handed participants (5 males and 5 females; mean age, 22.7 ± 2.4 years; range, 19–25) were recruited via advertisement. This number of participants has been established as sufficient for obtaining reliable parcellation results [Klein et al., 2007]. None of the participants had ever suffered from any psychiatric or neurological disease, and none had any contraindications for MRI scanning. All participants signed an informed consent form approved by the Medical Research Ethics Committee of Tianjin Medical University. For Datasets 2 and 3, 10 age- and gender-matched participants were selected from each of the databases.

Diffusion-Weighted Data Acquisition

All subjects in Dataset 1 were examined using a Signa HDx 3.0 Tesla MR scanner (General Electric, Milwaukee, WI). The diffusion tensor imaging (DTI) scheme contained 55 images with noncollinear diffusion gradients (b = 1000 s/mm^2) and 3 nondiffusion-weighted images (b = 0 s/mm^2) using a single-shot echo planar imaging sequence. An integrated parallel acquisition technique was used with an acceleration factor of 2 because acquisition time can be reduced by this technique, which also provides less image distortion from susceptibility artifacts. From each participant, 45 slices were collected with a field of view (FOV) = 256 × 256 mm, acquisition matrix = 128 × 128, flip angle (FA) = 90°, number of averages = 1, and slice thickness = 3 mm, with no gap. This method resulted in voxel-dimensions of 2 × 2 × 3

mm. The echo time (TE) was 64.2 ms and the repetition time (TR) was 10,000 ms. Sagittal 3D T1-weighted images were also acquired with a brain volume (BRAVO) sequence (TR/TE = 8.1/3.1 ms; inversion time = 450 ms; FA = 13°; FOV = 256 × 256 mm; matrix = 256 × 256; slice thickness = 1 mm, no gap; 176 sagittal slices).

For dataset 2, the DTI images consisted of 64 images with noncollinear diffusion gradients (b = 1000 s/mm^2) and 12 nondiffusion-weighted images (b = 0 s/mm^2). From each subject, 58 slices were collected with a FOV = 256 × 256 mm, acquisition matrix = 128 × 128, and slice thickness = 2 mm, with no gap. This method resulted in voxel-dimensions of 2 × 2 × 2 mm. The TE was 91 ms and TR 10,000 ms. 3D T1-weighted images were also acquired with the following parameters: (TR = 2500 ms, TE = 3.5 ms, FA = 8°, slice thickness = 1 mm, voxel resolution = 1 × 1 × 1 mm).

For dataset 3, the DTI images were acquired using a single-shot echo-planar imaging-based sequence with the following scanning parameters: 2.5 mm slice thickness with no gap, 49 axial slices, TR = 7200 ms, TE = 104 ms, acquisition matrix = 128 × 128, FOV = 230 × 230 mm, 64 diffusion directions with b = 1000 s/mm^2, and 1 nondiffusion-weighted image (b = 0 s/mm^2). Sagittal 3D T1-weighted images were also obtained (128 slices, TR = 2530 ms, TE = 3.39 ms, slice thickness = 1.33 mm, FA = 7°, inversion time [TI] = 1100 ms, FOV = 256 × 256 mm, in-plane resolution = 256 × 192).

Resting-State fMRI Data Acquisition

Resting-state fMRI data and T1-weighted images were collected for a different group of 29 healthy right-handed volunteers (18 males; age range = 18–44 years, mean age = 27.4 ± 6.3). To independently validate our parcellation results, this group did not overlap with the group in the diffusion-weighted imaging experiment. All participants gave informed written consent in accordance with ethical approval from the local ethics committee. The participants lay supine in a 3.0T Siemens MRI scanner. They were instructed to close their eyes and lie still. Cushions were used to reduce head motion. One hundred-eighty volumes of echo planar images were acquired using a gradient-echo single-shot echo planar imaging sequence (TR = 2000 ms, echo time = 30 ms; no gap; 40 axial slices with isotropic 3-mm voxels and a FOV = 240 × 240 mm^2). A structural scan was acquired for each participant in the same session, using a 3D T1 magnetization-prepared rapid acquisition gradient echo sequence (voxel size, 1 × 1 × 1 mm).

DTI Data Preprocessing

Both the DTI and T1-weighted data were visually inspected by two radiologists for obvious artifacts arising from subject motion and instrument malfunction. Distortions in the diffusion-weighted images caused by eddy-currents and simple head motions were then corrected using FMRIB's Diffusion Toolbox (FSL 4.0; http://www.fmrib.ox.ac.uk/fsl). Skull-stripped T1-weighted images from each participant were coregistered to the participant's non-diffusion-weighted image (b = 0 s/mm^2) using a statistical parametric mapping (SPM8) package (http://www.fil.ion.ucl.ac.uk/spm). This resulted in a set of coregistered T1 images in DTI space. Then the T1 images obtained in diffusion space were transformed to the Montreal Neurological Institute's 152-brain template (MNI152). Finally,

an inverse transformation was performed to transform the seed masks of the left STG and target masks into diffusion space for each subject. The same procedures were performed on the other two DTI datasets.

Resting-State fMRI Data Preprocessing

Preprocessing of the resting-state fMRI data was carried out using scripts provided by the 1000 Functional Connectomes Project (www.nitrc.org/projects/fcon_1000) [Biswal et al., 2010] using both FSL and AFNI (http://afni.nimh.nih.gov/afni) software. The preprocessing steps were: (1) discarding the first 10 volumes of each functional time series, correcting the slice timing for remaining images, and realigning them to the first volume to provide for head motion correction, (2) spatial smoothing with a Gaussian kernel of 6-mm full-width at half maximum, (3) removing linear trends and temporal band-pass filtering (0.01–0.08 Hz), (4) spatial normalization of the structural MR images to the MNI152 template, (5) coregistering the anatomical volume with the mean functional volume and regressing out nuisance signals such as those from cerebrospinal fluid and white matter as well as global signals and six motion parameters, and (6) resampling of the functional data into MNI space with the concatenated transformations. In the end, this preprocessing procedure provided a four-dimensional residual time series in standard MNI space for each participant.

Seed Mask Definition

The seed region of the left posterior STG was drawn on the left hemisphere of the MNI152 structural brain in MNI standard space (Fig. 1A). In the absence of detailed cytoarchitectonic measurements, it was necessary to use macroscopic boundaries that could be reliably identified as the boundaries of this region. A liberal mask was drawn that included the STG, part of the angular gyrus, the SMG, and the feet of the MTG, all areas which have been labeled as Wernicke's area in the literature [Bogen and Bogen, 1976; Wise et al., 2001]. The dorsal boundary of the seed region was the perisylvian fissure extending to the intermediate fissure of Jensen, and the ventral boundary was the superior temporal sulcus extending to the vertical cutting plane of Jensen's fissure. The anterior and posterior boundaries were hard to define, so we used a macroscopic sulcus or gyrus as the anatomical marker. The anterior border was formed by the postcentral sulcus vertically extending to the superior temporal sulcus, which is located lateral to the anterior boundary of Heschl's gyrus and the posterior border by the fissure of Jensen (Fig. 1A). The seed mask was then transformed into each participant's individual space using SPM8 software.

Probabilistic Tractography

Probabilistic tractography was performed in diffusion space using the FSL package. Probability distributions for two fiber directions at each voxel were calculated using multiple fiber extension [Behrens et al., 2007] from a previously published diffusion modeling approach [Behrens et al., 2003a, 2003b]. Drawing on these distributions, we estimated the fiber tracts between each voxel in the seed region and every voxel of the whole brain. Probabilistic tractography was applied by sampling 5000 streamline fibers per voxel to estimate the connectivity probability. Then, a small threshold value was used to threshold the path distribution estimates (10 out of 5,000 samples) [Makuuchi et al., 2009]. With this fixed arbitrary threshold we aimed at both reducing the false-positive connections

and retaining sufficient sensitivity to avoid missing the true connections [Heiervang et al., 2006; Johansen-Berg et al., 2007]. To facilitate data storage, all the connectivity profiles for each voxel were down-sampled to 5-mm isotropic voxels [Johansen-Berg et al., 2004]. Cross-correlations (dimensions: number of seeds × number of seeds) between the connectivity patterns of all voxels in the seed mask were calculated and used for automatic parcellation [Johansen-Berg et al., 2004]. The (*i*, *j*)th element value of the cross-correlation was defined by the correlation between the connectivity profile of seed *i* and the connectivity profile of seed *j*.

Tractography-Based Parcellation

The cross-correlation matrix was then fed into spectral clustering with edge-weighted centroidal Voronoi tessellation segmentation for automated clustering to define different clusters [Wang et al., 2012]. To avoid an arbitrary choice of the number of clusters, we used cross-validation to determine the number of clusters that yielded the optimal consistency across the three sets of data. In each set, we subdivided the posterior STG from 2 to 6 clusters in each subject. The maximum probability map for each subregion was created for different numbers of clusters across the 10 subjects in all three sets of data. To calculate the maximum probability map, we first transformed each individual parcellation result from the diffusion space to MNI space. Then the maximum probability map was calculated by assigning each voxel to the area in which it was most likely to be located. If two areas showed the same probability at a particular voxel, this voxel was assigned to the area with the higher average probabilities of the 26 voxels directly adjacent [Eickhoff et al., 2005]. The mean overlap degree characterized using Dice coefficient [Dice, 1945] and between the maximum probability maps of each cluster number across the three sets of data was calculated and was taken as the standard for choosing the optimal number of clusters. This analysis revealed a three-way parcellation as the most consistent solution, which was used to guide for further analyses. To facilitate the subsequent analyses, we extract the overlap part of each subregion of the maximum probability map across the three datasets for guiding the following analyses.

Whole-Brain Anatomical Connectivity Pattern

We mapped the whole brain anatomical connectivity for each cluster to identify its connectivity properties. To map the whole brain anatomical connectivity pattern for each subregion, we first transformed the seed masks to diffusion space, and probabilistic tracking was used to obtain the connectivity probability between each subregion and all the other voxels in the brain. We drew 5,000 samples from the connectivity distribution for each voxel and calculated the connection probability for each voxel. The identified fiber tracts were transformed into MNI space and all the connection probability maps were averaged to obtain a mean probability connectivity map for each subregion.

Anatomical Connectivity with Specific Target Brain Areas

We mapped the anatomical connections between each Wernicke’s subregion and Brodmann area (BA) 44, BA45 and precentral gyrus (PCG) to identify which subregion mainly connected to anterior frontal language areas. The target brain areas were defined using the

SPM Anatomy toolbox by calculating the maximum probability map of each target brain area [Eickhoff et al., 2005] (Fig. 2B). To compute the connectivity strength, we first extracted each subregion yielded by tractography-based parcellation and transformed the three subregions into diffusion space which served as the seed regions for tractography in each subject. Then, the anatomical connectivity between each seed area and each target brain area was mapped. For each subregion of Wernicke's area, we drew 5000 samples from the connectivity distribution for each voxel and calculated the connection probability between each subregion and each target brain area. Finally, we averaged all the connectivity probabilities across all subjects to acquire the mean connections.

Whole-Brain Resting-State Functional Connectivity Pattern

In this study, we used resting-state functional connectivity (RSFC) analyses to assess the functional network that each subregion participated in. First, seed masks were extracted from the overlap parts of maximum probability maps of all three datasets and sampled to 3-mm cubic voxels. Then, the mean time-courses of these masks were obtained. Finally, the whole-brain RSFC for each of the three clusters was calculated. The RSFC was defined by correlations between the time series. For each subject, the Pearson correlation coefficients between the mean time series of each seed region and those of each voxel of the whole brain were calculated and then converted to *z*-values using Fisher's *z* transformation to improve normality. Then each individual's *z*-values were entered into a random effect one-sample *t*-test in a voxel-wise manner to determine the regions that showed significant positive or negative correlations with the seed region. Moreover, a paired *t*-test was used to identify the exact regions that differed in their resting-state FC strengths between each pair of subregions. For all the above voxel-wise comparisons, the family wise error (FWE) method was used for multiple comparison correction ($P < 0.05$), and only clusters that contained a minimum of 30 voxels were reported.

Whole Brain Coactivation Connectivity Pattern

In this study, the task-dependent coactivated functional connectivity of each subregion was mapped using meta-analytic connectivity modeling (MACM) approaches [Eickhoff et al., 2010; Laird et al., 2013; Robinson et al., 2010] in the BrainMap database [Laird et al., 2011; Laird et al., 2009a]. The main procedure of MACM analyses are as follows. First, we retrieved for each of the subregions yielded by tractography-based parcellation all studies from the BrainMap database that reported activation within that particular subregion. Note that we considered all eligible BrainMap experiments because any preselection based on taxonomic categories would have constituted a strong a priori hypothesis about how brain networks are organized. However, it remains elusive how well psychological constructs, such as emotion and cognition, map on regional brain responses [Bzdok et al., 2014]. In other words, experiments were defined purely based on location not by the type of experiment or contrast they probe to yield unbiased maps of whole-brain coactivation. In turn, the subsequent functional characterization then probes the type of paradigm classes and behavioral domains featured by the experiments activating each subregion. Subsequently, activation likelihood estimation (ALE) meta-analysis was performed on the sets of coordinates to establish which brain regions were significantly coactivated with a particular subregion. Using ALE, the identified coordinates were modeled with a three-dimensional

Gaussian distribution, and their convergence across experiments was quantitatively assessed [Laird et al., 2009b]. The ALE score for the MACM analysis of each cluster was compared to a null-distribution that reflected a random spatial association between experiments with a fixed within-experiment distribution of foci [Eickhoff et al., 2009]. This random-effects inference assesses the above-chance convergence between experiments instead of the clustering of foci within a particular experiment. The observed ALE scores from the actual meta-analysis of experiments activated within a particular subregion were then tested against the ALE scores obtained under this null-distribution yielding a *P*-value based on the proportion of equal or higher random values [Eickhoff et al., 2012]. These nonparametric *P*-values were converted to z-scores and thresholded at $P < 0.05$ (cluster-level FWE-corrected, cluster-forming threshold at voxel-level $P < 0.001$). In addition, contrast analyses between each subregion were performed to show the distinction of coactivation functional connectivity maps. First, the coactivation connectivity map of each cluster was computed using MACM. Then, the difference analysis on each pair of coactivation maps was performed and the voxels that were significantly more likely coactivated with either cluster were retained.

Conjunction of Resting and Coactivation Network

We mapped the overlap networks formed by the overlapping the resting-state and coactivation networks to identify the shared connectivities of resting and task state, which assess the functional network characteristics from complementary perspectives. To calculate the conjunction network, we first obtained the whole brain resting-state functional and coactivation networks, as described above. Then, the overlap between the two networks was calculated for each subregion.

Behavioral Domain Analysis

Functional characterization of each subregion was determined using forward inferences to determine the main functions associated with each subregion yielded by tractography-based parcellation [Bzdok et al., 2013; Clos et al., 2013]. The behavioral domain analysis results include five behavior domains (action, cognition, emotion, interoception, and perception) and 51 behavioral subdomains. Forward inference represents the probability of observing activity in a brain region given knowledge of the psychological process. In the forward inference approach, a subregion's functional profile was determined by identifying the taxonomic labels (domains or subdomains) for which the probability of finding activation in a specific subregion was significantly higher than the overall chance (across the entire database) of finding activation in that particular subregion. Significance was established using a binomial test [$P < 0.05$ corrected for multiple comparisons using false discovery rate (FDR) method] [Eickhoff et al., 2011].

Meta-Analyses of Semantics, Execution Speech, and Phonology in Wernicke's Area

To further test which subregion was mainly involved in language processing, we performed meta-analyses of semantics, execution speech and phonology which have been widely reported to activate the posterior STG in the BrainMap database. We used the Wernicke's area mask defined in this study as the seed region and searched the related articles which

reported activation foci in this region. The search criteria as follows: the behavior domain was semantics, execution speech and phonology; the imaging modality was fMRI or positron emission tomography (PET); and the experiment content was normal mapping. No further constraints were applied.

Meta-analysis of semantics identified 15 papers, 23 experiments. Meta-analysis of execution speech identified 18 papers, 25 experiments, and meta-analysis of phonology identified 42 papers, 144 experiments. Then, we performed ALE for Wernicke's area and segmented the ALE maps into three different clusters according to the three subregions yielded by tractography-based parcellation to identify which subregions were involved in these functions.

Intraoperative Electrical Stimulation of the Posterior STG

Participants—To localize the most relevant brain sites for language processing in the defined posterior STG, intraoperative electrical stimulation was used during tumor resection in two glioma patients. Both patient 1 (P1) (aged 33) and patient 2 (P2) (aged 32) were males. In P1, the glioma was located on the left inferior parietal lobule, whereas in P2, it was located on the middle part of the left middle and inferior temporal gyrus. Preoperatively, both patients had a neurological examination. Their language was tested by a speech therapist to ascertain that neither of the patients had any language disorders, especially anomia. And both participants signed an informed consent.

Intraoperative Electrical Stimulation Mapping

The two patients underwent neurosurgery under local anesthesia, so functional cortical mapping could be carried out using direct electrical stimulation. A bipolar electrode with 5 mm between the tips (pulse frequency, 60 Hz; pulse duration, 1ms; pulse amplitude, 2–8 mA) was applied to the cortex structures in the awake patients. When their language-related regions were stimulated at certain intensity, the process of language production was disturbed, and the patient showed speech arrest/anomia, or other types of language disorders [Ojemann, 1983]. The electrical stimulation was synchronized with the linguistic task which was presented for up to 4,000 ms. In this study, we used an object picture-naming task to identify the brain sites most involved in language processing [Ojemann et al., 1989]. Stimulation was applied to different regions including posterior STG and temporoparietal junction (TPJ) area and the patient was asked to name the object in the picture at the same time. The most relevant brain sites were identified when patients showed anomia or speech arrest. In P1, the positive response site in the posterior STG was found and marked as #16. In P2, two relevant sites were identified and marked as #2 and #3 in the posterior STG.

RESULTS

Connectivity-Based Parcellation of the Left Posterior STG

In this study, we used in vivo probabilistic tractography and a clustering algorithm to parcellate the left posterior STG into distinct components defined by their unique structural connections with the rest of the brain in the individual space for each subject in three sets of data. As the actual number of clusters was unknown, we used a multicenter-based method to

determine the ultimate number of clusters by calculating the average degree of overlap between the maximum probability maps yielded by tractography-based parcellation of the three datasets. The optimal number of parcels for left posterior STG was estimated to be 3, which resulted in the highest Dice's coefficient between clustering solutions (Fig. 1B). Therefore, we selected a three-way parcellation scheme for the left posterior STG. In the subsequent analyses, the overlap parts of maximum probability maps of all three datasets were used for further analysis (Fig. 1C).

Grouping the voxels into three clusters resulted in an anterior cluster located lateral to the transverse temporal gyrus. The other two subregions included a middle cluster that approximately corresponded to the planum temporale and a posterior cluster at the conjunction of the ventral parietal cortex, caudal STG, and base of the MTG corresponding to the left TPJ area.

Whole Brain Structural Connectivity

We mapped the whole brain structural connectivity for each subregion to reveal different anatomical connectivity patterns for each subregion (Fig. 2A). The primary anatomical connections for the most anterior subregion (Cluster 1) were found in the ventral and dorsal premotor cortex (PMv and PMd), postcentral gyrus, SMG, angular gyrus (AG), insula (IN), and inferior frontal gyrus (IFG) via the superior longitudinal fasciculus (SLF) III and arcuate fasciculus (AF) [Makris et al., 2005]. The middle subregion (Cluster 2) primarily connected with posterior MTG, SMG, AG, postcentral gyrus, PMv, IN, and IFG. The main white matter pathways connecting the middle subregion with these brain areas are also SLF III and AF. The most posterior subregion (Cluster 3) mainly connected with MTG, inferior temporal gyrus (ITG), SMG, AG, IN, superior parietal lobule (SPL), precuneus and PMv. The main white matter pathways are SLF III, AF, and extreme capsule (EmC) [Makris and Pandya, 2009].

In addition, to quantify the anatomical connectivity strength between each Wernicke's subregion and anterior frontal language areas, we calculated the anatomical connectivity probability between each subregion and BA44, BA45, and PCG. The anatomical connectivity analyses revealed that the two anterior subregions have stronger anatomical connectivity strength with BA44 and BA45 than the most posterior subregion located in the TPJ area (Fig. 2C).

Whole-Brain RSFC Pattern

We performed whole-brain RSFC analyses to determine which cortical network is associated with each of the three clusters. RSFC analyses revealed that the two anterior subregions primarily participated in language network, whereas the most posterior subregion participated in default model network (Fig. 3).

Positively-Correlated Networks

Cluster 1 was primarily correlated with bilateral Broca's area, the bilateral STG, left PCG, bilateral postcentral gyrus, bilateral supplementary motor area, bilateral middle cingulate gyrus, bilateral SMG and right posterior MTG. Cluster 2 predominantly showed FC with the

left anterior precuneus, bilateral posterior MTG, left Broca's area, left frontal pole, left temporal pole, and bilateral SMG. Cluster 3 primarily showed functional connections with the left temporal pole, bilateral MTG, bilateral dorsolateral pre-frontal cortex, bilateral superior frontal gyrus, bilateral precuneus, and bilateral medial prefrontal cortex (Fig. 3).

Anticorrelated Networks

In addition to the positive RSFCs, negative RSFCs were also identified. Cluster 1 was primarily negatively correlated with the left anterior MTG, bilateral superior frontal gyrus, bilateral dorsolateral prefrontal cortex, bilateral angular gyrus, right frontal pole, and bilateral posterior precuneus. For Cluster 2, the primarily negative RSFCs were identified in the right intraparietal sulcus and bilateral primary visual cortex. Cluster 3 was primarily negatively correlated with the right Broca's area and bilateral primary visual cortex (Fig. 3).

Variations in Functional Connectivity between Clusters

Statistical analyses revealed significant connectivity differences between each subregion in the left posterior STG (Fig. 3), which confirmed that the different subregions had different functional connectivity patterns.

Whole Brain Coactivation Connectivity Pattern

MACM was used to determine the task-dependent coactivated FC pattern for each subregion in the left posterior STG. This revealed that both anterior clusters, Clusters 1 and 2, were main components of the language network (Fig. 4). For Cluster 1, the coactivated brain regions included bilateral Broca's area, bilateral the supplementary motor area, bilateral ventral premotor cortex, bilateral cerebellum, bilateral STG, and bilateral anterior insula. The coactivated connectivity pattern for Cluster 2 was similar to that of Cluster 1. Cluster 2 was primarily coactivated with the bilateral Broca's area, bilateral supplementary motor area, bilateral ventral premotor cortex, bilateral posterior MTG, and bilateral anterior insula. Unlike Cluster 1, no brain regions from Cluster 2 were coactivated with the middle STG. The coactivated task-dependent FC pattern for Cluster 3 was characterized by connections with the bilateral insula, bilateral dorsal prefrontal gyrus, left posterior MTG, and right posterior TPJ area (Fig. 4). Additionally, the contrast analyses between each pair of subregions were performed to determine the different coactivation connectivity patterns. Contrast analyses revealed different coactivation connectivity of each subregion of the left posterior STG (Fig. 4).

Overlap Network between Resting and Coactivation Networks

We also mapped the overlap network shared by both resting-state connectivity and task-dependent coactivation connectivity to collectedly reveal the cortical network that each subregion participated in. The overall network for Cluster 1 includes bilateral STG, bilateral ventral premotor cortex, and left Broca's area and left dorsal premotor cortex. For Cluster 2, the overall network includes left Broca's area and right posterior MTG. The overall network work for Cluster 3 was found to mainly connect with right posterior TPJ area (Fig. 5).

Behavioral Domain Analysis

Functional characterization of each Wernicke's area yielded by tractography-based parcellation revealed that the most anterior subregion (Cluster 1) primarily participated in audition perception, music, phonology, and speech. The middle subregion (Cluster 2) was found to be mainly involved in language speech, whereas most posterior subregion (Cluster 3) was primarily involved in social cognition (Fig. 6).

Meta-Analyses of Semantics, Execution Speech and Phonology

We performed a meta-analysis of semantic processing, execution speech and phonology to determine which subregions participate in these language-related functions. ALE was performed, and ALE map for each function was segmented into three clusters according to the three subregions yielded by tractography-based parcellation (Fig. 7). Meta-analysis also revealed that the anterior two clusters were predominantly involved in semantic processing, execution speech and phonology. This result further confirmed the previous findings.

Intraoperative Electrical Stimulation Mapping

Finally, we applied cortical mapping using intraoperative electrical stimulation to exactly localize the most relevant sites for language processing in the defined posterior STG. Intraoperative electrical stimulation revealed areas which were clearly specific for object picture-naming in the two glioma patients. In P1, speech arrest occurred with stimulation at the area marked by #16 in the posterior STG. This area corresponded well to Cluster 2 in the tractography-based parcellation. In P2, three sites were identified as the most relevant to object picture-naming performance. One site (#1) was located in the superior temporal sulcus. The other two (#2 and #3) were located on the posterior STG, corresponding to Clusters 1 and 2, respectively (Fig. 8). The intraoperative electrical stimulation mapping indicated that the Wernicke's area only included the two anterior subregions.

DISCUSSION

The goal of this study was to explore the possibility that the cortical expanse of the left posterior STG can be subdivided on the basis of structural connectivity patterns to identify the posterior anatomical border of Wernicke's area. Three subregions with distinct connectivity patterns were identified consistently in three different datasets. The anatomical connectivity, RSFC and task-dependent coactivated pattern analyses for each subregion yielded by tractography-based parcellation demonstrated that "Wernicke's area" is located on the posterior STG, but does not include the TPJ area. Moreover, we used behavioral domain analysis, meta-analyses of semantics, execution speech and phonology and intraoperative electrical stimulation technique to further validate the anatomical connectivity, RSFC and MACM findings. These complementary approaches consistently identified the posterior anatomical border of Wernicke's area.

The question of the location of Wernicke's area has puzzled researchers for more than a century. Wernicke's area was first defined by the German neurologist Carl Wernicke based on the fact that brain lesions in or around the posterior STG resulted in "Wernicke's aphasia." Subsequently, various anatomical boundaries of Wernicke's area were proposed to

delineate its anatomical location and were chosen to investigate its function or connectivity [Bogen and Bogen, 1976; Brodmann, 1909; Geschwind, 1970; Mesulam, 1998; Parker et al., 2005; Pataraia et al., 2005; Rauschecker and Scott, 2009a; Ross, 2010; Tomasi and Volkow, 2012]. A recent meta-analysis study established a role for the anterior STG in auditory word-form recognition, a finding which implied that Wernicke's area might be located on the anterior STG [Dewitt and Rauschecker, 2012]. The discrepancies between the definitions of Wernicke's area may have primarily resulted from various phenotypes of "Wernicke's aphasia." In the absence of clear definitions of either its functions or its anatomical boundaries, Wernicke's area even has been considered to be a relatively meaningless concept [Bogen and Bogen, 1976]. Some studies tried to define Wernicke's area using task-dependent neuroimaging and lesion-based mapping techniques [Abrams et al., 2013; Boatman et al., 2000a]. However, task-based neuroimaging cannot explicitly discriminate the border of functional subregions, and functional imaging may produce misleading activations for localizing cognitive-behavioral functions [Ross, 2010]. Lesion-based mapping also cannot definitely determine the function of a brain area if it contains multiple subregions that each contribute to the altered behavior [Bates et al., 2003]. Therefore, the anatomical boundary of Wernicke's area has continued to be an open question. In our study, we proposed to address this question from a new perspective that utilized connectivity-based parcellation to identify functional subregions to determine which subregions belong to Wernicke's area. This shed a new light on this question from a new avenue.

Many techniques, such as cytoarchitecture [Schleicher et al., 1999], myeloarchitecture [Glasser and Van Essen, 2011], and receptor distribution pattern [Geyer et al., 1996], have been developed to delineate the subregions of various brain areas. However, although these measurements reflect detailed local organization of cortical areas at the microscale, they cannot provide connectivity information, especially long-range connectivity, which is essential for determining the functions that an area can perform. Anatomical connectivity-based parcellation of Wernicke's area by characterizing the interplay between its subregions and other brain areas to define functional subregions could better inform our understanding of its functional segregation and guide the interpretation of its functions [Averbeck et al., 2009; Passing-ham et al., 2002]. Compared with structural covariance patterns and RSFC patterns, anatomical connectivity pattern is more reliable and reproducible. Recently, using anatomical connectivity patterns-based parcellation approach, right TPJ whose boundary is also unclear was parcellated into different subregions, and the exact functional subnetworks were identified [Mars et al., 2012]. In our current study, different functional subareas were identified suggesting that differential anatomical subregions can be effectively defined on the basis of estimated anatomical connectivity. Diffusion-tractography parcellation and the subsequent connectivity analyses provided independent and convergent evidence about the subregions that belong to Wernicke's area.

Emerging evidence has demonstrated that Wernicke's area and Broca's area are anatomically connected by direct white matter pathway [Friederici, 2009; Geschwind, 1972]. The anatomical connectivity analyses in the current study found that the two anterior subregions have stronger connections with BA44 and BA45 than the most posterior subregion, which suggested that Wernicke's area might be only located on posterior STG. RSFC, which primarily reflects brain spontaneous fluctuations, can reveal the task-

independent intrinsic functional cortical network of the brain [Biswal et al., 1995], whereas MACM primarily looks for global coactivation patterns across a diverse range of tasks to reveal the task-dependent functional network [Laird et al., 2009b; Turkeltaub et al., 2002]. In the current study, both RSFC and MACM analyses revealed that the two anterior subregions located on the posterior STG primarily participated in language networks, whereas the most posterior subregion located on the TPJ area was predominantly coupled with the default mode network, as revealed by RSFC analyses [Raichle et al., 2001]. The different cortical functional networks of each subregion revealed using RSFC and MACM demonstrated that the "Wernicke's area" was primarily located on the posterior STG not including the TPJ area. Moreover, the RSFC of the most anterior subregion, Cluster 1, suggested that this area might be simultaneously involved in speech perception [Cohen et al., 2002; Dehaene-Lambertz et al., 2002; Fiez et al., 1996; Friederici, 2002; Geschwind, 1965; Hickok, 2001; Mummery et al., 1999; Obleser et al., 2007; Rauschecker and Scott, 2009b] and production [Dhanjal et al., 2008; Fiez et al., 1996; Hickok, 2001; Turkeltaub et al., 2002], which was confirmed by the subsequent behavioral domain analysis for this subregion. In addition, the RSFC and MACM analyses showed that Cluster 1 has more connections with the anterior and contralateral STG, a finding which may suggest that the most anterior subregion is more associated with the integration of phonemes into temporally complex patterns [Dewitt and Rauschecker, 2012] and more dedicated to language semantic processing [Friederici, 2009; Saur et al., 2008].

Wernicke's area is traditionally associated with language comprehension. Recent studies suggested that Wernicke's area may be also involved in speech perception and production [Hickok and Poeppel, 2004], decoding discourse semantics [Tanner, 2007], auditory word-form recognition and inner speech [DeWitt and Rauschecker, 2013]. The functional diversity of Wernicke's area indicated that Wernicke's area is not a homogenous area but participates in various language-related functions. Functional characterization of each subregion yielded by tractography-based parcellation using behavioral domain analyses revealed that the two anterior subregions participated in different language-related functions. The most anterior subregion primarily participated in audition perception, which was supported by both resting-state and task-related connectivity analyses identifying specific connectivity with bilateral STG. The middle subregion Cluster 2 primarily participated in language speech, whereas the most posterior subregion primarily participated in social cognition. This functional characterization of each subregion indicated that only subregions located in the posterior STG belong to Wernicke's area and demonstrated that Wernicke's area is a functionally heterogeneous area. The behavioral analysis results for each subregion were consistent with the RSFC and MACM findings and was supported by our intraoperative electrical mapping and the previous lesion-based mapping results that language processing was most related to posterior STG [Ojemann, 1983, 1991]. Furthermore, the behavioral domain and functional connectivity analyses for the most posterior subregion was consistent with that of the right TPJ subarea (TPJp), which was also discovered to be predominantly involved in social cognition and coupled with the default mode network [Mars et al., 2012]. Our resting-state and task-dependent mapping collectively revealed the connectivity with the right TPJp, which further indicating the functional coupling between left and right TPJ. The discrepancy between our findings and

previous functional role of TPJ maybe result from lacking of exact functional and anatomical study for this area at a finer scale. Recently, function-based parcellation of angular gyrus revealed that the anterior angular mainly participated in default model network, whereas the posterior ventral angular gyrus is involved in semantic processing [Seghier et al., 2010]. Considering the anatomical segregation from traditionally defined Wernicke's area, we argued that angular gyrus may not belong to Wernicke's area. And it may be another semantic processing center as Wernicke's area [Joseph, 1982; Seghier, 2013].

The constructed atlas of Wernicke's area could improve our future language-related studies, especially for the clinical Wernicke's aphasia. The atlas of Wernicke's area was calculated in standard MNI space and has the same dimensions as the nonlinear average template in MNI space (MNI152_T1_1mm_ brain: 181 × 217 × 181 voxels, 1 × 1 × 1 mm/voxel). Therefore, using registration method with commonly used software such as SPM and FSL, this atlas can be transformed into individual subject's brain in other datasets to investigate its connectivity and function. Furthermore, the constructed atlas of this area will be uploaded into our lab website (http://atlas.brainnetome.org/) for downloading.

The present methodological limitation is that all of the brains in different datasets have to be transformed from individual diffusion space to MNI space to calculate the statistic maximum probability map (MPM). However, the registration problem is hard to be settled in human neuroimaging studies because of great individual differences. In our current study, we utilized high resolution structural MRI to transform the brain images in diffusion space into MNI space to improve the accuracy of registration. Moreover, we calculated the overlap of the MPM across the three populations to guide the subsequent analyses to further ameliorate the registration error to guarantee our present study reliable.

In summary, our results demonstrated that the posterior Wernicke's area is located on the posterior STG but does not include the TPJ area. The identified anatomical boundary of Wernicke's area was further validated by resting-state and task-dependent coactivation connectivity analyses, and behavioral domain analyses. This redefinition of the anatomical boundary of Wernicke's area could facilitate future studies on this area by enabling them to investigate the area using a more fine-grained approach. The functional characterization of its subregions provides new insights about the functional organization of Wernicke's area.

Acknowledgments

Contract grant sponsor: National Basic Research Program of China; Contract grant number: 973 program; 2012CB720702, 2011CB707801; Contract grant sponsor: Strategic Priority Research Program of the Chinese Academy of Sciences; Contract grant number: XDB02030300; Contract grant sponsor: Natural Science Foundation of China; Contract grant number: 91132301

The authors thank Rhoda E. and Edmund F. Perozzi for editing assistance and Yanchao Bi for useful suggestions.

References

Abrams DA, Ryali S, Chen T, Balaban E, Levitin DJ, Menon V. Multivariate activation and connectivity patterns discriminate speech intelligibility in Wernicke's, Broca's, and Geschwind's areas. Cereb Cortex. 2013; 23:1703–1714. [PubMed: 22693339]

Averbeck BB, Battaglia-Mayer A, Guglielmo C, Caminiti R. Statistical analysis of parieto-frontal cognitive-motor networks. J Neurophysiol. 2009; 102:1911–1920. [PubMed: 19625537]

Bates E, Wilson SM, Saygin AP, Dick F, Sereno MI, Knight RT, Dronkers NF. Voxel-based lesion-symptom mapping. Nat Neurosci. 2003; 6:448–450. [PubMed: 12704393]

Behrens TE, Berg HJ, Jbabdi S, Rushworth MF, Woolrich MW. Probabilistic diffusion tractography with multiple fibre orientations: What can we gain? Neuroimage. 2007; 34:144–155. [PubMed: 17070705]

Behrens TE, Johansen-Berg H, Woolrich MW, Smith SM, Wheeler-Kingshott CA, Boulby PA, Barker GJ, Sillery EL, Sheehan K, Ciccarelli O, Thompson AJ, Brady JM, Matthews PM. Non-invasive mapping of connections between human thalamus and cortex using diffusion imaging. Nat Neurosci. 2003a; 6:750–7. [PubMed: 12808459]

Behrens TE, Woolrich MW, Jenkinson M, Johansen-Berg H, Nunes RG, Clare S, Matthews PM, Brady JM, Smith SM. Characterization and propagation of uncertainty in diffusion-weighted MR imaging. Magn Reson Med. 2003b; 50:1077–1088. [PubMed: 14587019]

Binder JR, Frost JA, Hammeke TA, Bellgowan PS, Springer JA, Kaufman JN, Possing ET. Human temporal lobe activation by speech and nonspeech sounds. Cereb Cortex. 2000; 10:512–28. [PubMed: 10847601]

Biswal B, Yetkin FZ, Haughton VM, Hyde JS. Functional connectivity in the motor cortex of resting human brain using echo-planar MRI. Magn Reson Med. 1995; 34:537–41. [PubMed: 8524021]

Biswal BB, Mennes M, Zuo XN, Gohel S, Kelly C, Smith SM, Beckmann CF, Adelstein JS, Buckner RL, Colcombe S, Dogonowski AM, Ernst M, Fair D, Hampson M, Hoptman MJ, Hyde JS, Kiviniemi VJ, Kotter R, Li SJ, Lin CP, Lowe MJ, Mackay C, Madden DJ, Madsen KH, Margulies DS, Mayberg HS, McMahon K, Monk CS, Mostofsky SH, Nagel BJ, Pekar JJ, Peltier SJ, Petersen SE, Riedl V, Rombouts SA, Rypma B, Schlaggar BL, Schmidt S, Seidler RD, Siegle GJ, Sorg C, Teng GJ, Veijola J, Villringer A, Walter M, Wang L, Weng XC, Whitfield-Gabrieli S, Williamson P, Windischberger C, Zang YF, Zhang HY, Castellanos FX, Milham MP. Toward discovery science of human brain function. Proc Natl Acad Sci USA. 2010; 107:4734–4739. [PubMed: 20176931]

Blank SC, Scott SK, Murphy K, Warburton E, Wise RJ. Speech production: Wernicke, Broca and beyond. Brain. 2002; 125:1829–1838. [PubMed: 12135973]

Boatman D, Gordon B, Hart J, Selnes O, Miglioretti D, Lenz F. Transcortical sensory aphasia: Revisited and revised. Brain Lang. 2000a; 123(Pt 8):1634–1642.

Boatman D, Gordon B, Hart J, Selnes O, Miglioretti D, Lenz F. Transcortical sensory aphasia: Revisited and revised. Brain. 2000b; 123(Pt 8):1634–1642. [PubMed: 10908193]

Bogen JE, Bogen GM. Wernicke's region—Where is it? Ann N Y Acad Sci. 1976; 280:834–843. [PubMed: 1070943]

Brodmann, K. Vergleichende Lokalisationslehre der Grobhirnrinde. Leipzig; Barth: 1909.

Buchsbaum BR, Hickok G, Humphries C. Role of left posterior superior temporal gyrus in phonological processing for speech perception and production. Cognit Sci. 2001; 25:663–678.

Bzdok D, Laird AR, Zilles K, Fox PT, Eickhoff SB. An investigation of the structural, connectional, and functional subspecialization in the human amygdala. Hum Brain Mapp. 2013; 34:3247–3266. [PubMed: 22806915]

Bzdok D, Heeger A, Langner R, Laird AR, Fox PT, Palomero-Gallagher N, Vogt BA, Zilles K, Eickhoff SB. Subspecialization in the human posterior medial cortex. Neuroimage. 2014; 106C: 55–71. [PubMed: 25462801]

Clos M, Amunts K, Laird AR, Fox PT, Eickhoff SB. Tackling the multifunctional nature of Broca's region meta-analytically: Co-activation-based parcellation of area 44. Neuroimage. 2013; 83:174–88. [PubMed: 23791915]

Cohen L, Lehericy S, Chochon F, Lemer C, Rivaud S, Dehaene S. Language-specific tuning of visual cortex? Functional properties of the Visual Word Form Area. Brain. 2002; 125:1054–1069. [PubMed: 11960895]

Cohen MX, Schoene-Bake JC, Elger CE, Weber B. Connectivity-based segregation of the human striatum predicts personality characteristics. Nat Neurosci. 2009; 12:32–34. [PubMed: 19029888]

Dehaene-Lambertz G, Dehaene S, Hertz-Pannier L. Functional neuroimaging of speech perception in infants. Science. 2002; 298:2013–2015. [PubMed: 12471265]

Dewitt I, Rauschecker JP. Phoneme and word recognition in the auditory ventral stream. Proc Natl Acad Sci USA. 2012; 109:E505–E514. [PubMed: 22308358]

DeWitt I, Rauschecker JP. Wernicke's area revisited: Parallel streams and word processing. Brain Lang. 2013; 127:181–191. [PubMed: 24404576]

Dhanjal NS, Handunnetthi L, Patel MC, Wise RJ. Perceptual systems controlling speech production. J Neurosci. 2008; 28:9969–9975. [PubMed: 18829954]

Dice LR. Measures of the amount of ecologic association between species. Ecology. 1945; 26:297–302.

Eickhoff SB, Stephan KE, Mohlberg H, Grefkes C, Fink GR, Amunts K, Zilles K. A new SPM toolbox for combining probabilistic cytoarchitectonic maps and functional imaging data. Neuroimage. 2005; 25:1325–1335. [PubMed: 15850749]

Eickhoff SB, Laird AR, Grefkes C, Wang LE, Zilles K, Fox PT. Coordinate-based activation likelihood estimation meta-analysis of neuroimaging data: A random-effects approach based on empirical estimates of spatial uncertainty. Hum Brain Mapp. 2009; 30:2907–2926. [PubMed: 19172646]

Eickhoff SB, Jbabdi S, Caspers S, Laird AR, Fox PT, Zilles K, Behrens TE. Anatomical and functional connectivity of cytoarchitectonic areas within the human parietal operculum. J Neurosci. 2010; 30:6409–6421. [PubMed: 20445067]

Eickhoff SB, Bzdok D, Laird AR, Roski C, Caspers S, Zilles K, Fox PT. Co-activation patterns distinguish cortical modules, their connectivity and functional differentiation. Neuroimage. 2011; 57:938–949. [PubMed: 21609770]

Eickhoff SB, Bzdok D, Laird AR, Kurth F, Fox PT. Activation likelihood estimation meta-analysis revisited. Neuroimage. 2012; 59:2349–2361. [PubMed: 21963913]

Fan L, Wang J, Zhang Y, Han W, Yu C, Jiang T. Connectivity-based parcellation of the human temporal pole using diffusion tensor imaging. Cereb Cortex. 2014; 24:3365–3378. [PubMed: 23926116]

Fiez JA, Raichle ME, Balota DA, Tallal P, Petersen SE. PET activation of posterior temporal regions during auditory word presentation and verb generation. Cereb Cortex. 1996; 6:1–10. [PubMed: 8670633]

Friederici AD. Towards a neural basis of auditory sentence processing. Trends Cognit Sci. 2002; 6:78–84. [PubMed: 15866191]

Friederici AD. Pathways to language: Fiber tracts in the human brain. Trends Cognit Sci. 2009; 13:175–81. [PubMed: 19223226]

Geschwind N. Disconnexion syndromes in animals and man. I. Brain. 1965; 88:237–294. [PubMed: 5318481]

Geschwind N. The organization of language and the brain. Science. 1970; 170:940–944. [PubMed: 5475022]

Geschwind N. Language and the brain. Sci Am. 1972; 226:76–83. [PubMed: 5014017]

Geyer S, Ledberg A, Schleicher A, Kinomura S, Schormann T, Burgel U, Klingberg T, Larsson J, Zilles K, Roland PE. Two different areas within the primary motor cortex of man. Nature. 1996; 382:805–807. [PubMed: 8752272]

Glasser MF, Van Essen DC. Mapping human cortical areas in vivo based on myelin content as revealed by T1- and T2-weighted MRI. J Neurosci. 2011; 31:11597–11616. [PubMed: 21832190]

Heiervang E, Behrens TE, Mackay CE, Robson MD, Johansen-Berg H. Between session reproducibility and between subject variability of diffusion MR and tractography measures. Neuroimage. 2006; 33:867–77. [PubMed: 17000119]

Hickok G. Functional anatomy of speech perception and speech production: Psycholinguistic implications. J Psycholinguist Res. 2001; 30:225–235. [PubMed: 11523272]

Hickok G, Poeppel D. Towards a functional neuroanatomy of speech perception. Trends Cogn Sci. 2000; 4:131–138. [PubMed: 10740277]

Hickok G, Poeppel D. Dorsal and ventral streams: A framework for understanding aspects of the functional anatomy of language. Cognition. 2004; 92:67–99. [PubMed: 15037127]

Johansen-Berg H, Behrens TE, Robson MD, Drobnjak I, Rushworth MF, Brady JM, Smith SM, Higham DJ, Matthews PM. Changes in connectivity profiles define functionally distinct regions in human medial frontal cortex. Proc Natl Acad Sci USA. 2004; 101:13335–13340. [PubMed: 15340158]

Johansen-Berg H, Della-Maggiore V, Behrens TE, Smith SM, Paus T. Integrity of white matter in the corpus callosum correlates with bimanual co-ordination skills. Neuroimage. 2007; 36(Suppl 2):T16–T21. [PubMed: 17499163]

Joseph R. The neuropsychology of development hemispheric laterality, limbic language, and the origin of thought. J Clin Psychol. 1982; 38:4–33. [PubMed: 7056873]

Klein JC, Behrens TE, Robson MD, Mackay CE, Higham DJ, Johansen-Berg H. Connectivity-based parcellation of human cortex using diffusion MRI: Establishing reproducibility, validity and observer independence in BA 44/45 and SMA/pre-SMA. Neuroimage. 2007; 34:204–211. [PubMed: 17023184]

Laird AR, Eickhoff SB, Kurth F, Fox PM, Uecker AM, Turner JA, Robinson JL, Lancaster JL, Fox PT. ALE meta-analysis workflows via the brainmap database: Progress towards a probabilistic functional brain atlas. Front Neuroinform. 2009a; 3:23. [PubMed: 19636392]

Laird AR, Eickhoff SB, Li K, Robin DA, Glahn DC, Fox PT. Investigating the functional heterogeneity of the default mode network using coordinate-based meta-analytic modeling. J Neurosci. 2009b; 29:14496–14505. [PubMed: 19923283]

Laird AR, Eickhoff SB, Fox PM, Uecker AM, Ray KL, Saenz JJ Jr, McKay DR, Bzdok D, Laird RW, Robinson JL, Turner JA, Turkeltaub PE, Lancaster JL, Fox PT. The BrainMap strategy for standardization, sharing, and meta-analysis of neuroimaging data. BMC Res Notes. 2011; 4:349. [PubMed: 21906305]

Laird AR, Eickhoff SB, Rottschy C, Bzdok D, Ray KL, Fox PT. Networks of task co-activations. Neuroimage. 2013; 80:505–514. [PubMed: 23631994]

Li W, Qin W, Liu H, Fan L, Wang J, Jiang T, Yu C. Subregions of the human superior frontal gyrus and their connections. Neuroimage. 2013; 78:46–58. [PubMed: 23587692]

Liu H, Qin W, Li W, Fan L, Wang J, Jiang T, Yu C. Connectivity-based parcellation of the human frontal pole with diffusion tensor imaging. J Neurosci. 2013; 33:6782–6790. [PubMed: 23595737]

Makris N, Pandya DN. The extreme capsule in humans and rethinking of the language circuitry. Brain Struct Funct. 2009; 213:343–358. [PubMed: 19104833]

Makris N, Kennedy DN, McInerney S, Sorensen AG, Wang R, Caviness VS Jr, Pandya DN. Segmentation of subcomponents within the superior longitudinal fascicle in humans: A quantitative, in vivo, DT-MRI study. Cereb Cortex. 2005; 15:854–869. [PubMed: 15590909]

Makuuchi M, Bahlmann J, Anwander A, Friederici AD. Segregating the core computational faculty of human language from working memory. Proc Natl Acad Sci USA. 2009; 106:8362–8367. [PubMed: 19416819]

Mars RB, Sallet J, Schuffelgen U, Jbabdi S, Toni I, Rushworth MF. Connectivity-based subdivisions of the human right “temporoparietal junction area”: Evidence for different areas participating in different cortical networks. Cereb Cortex. 2012; 22:1894–903. [PubMed: 21955921]

Mason RA, Prat CS, Just MA. Neurocognitive Brain Response to Transient Impairment of Wernicke’s Area. Cereb Cortex. 2014; 24:1474–1484. [PubMed: 23322403]

Mesulam MM. From sensation to cognition. Brain. 1998; 121(Pt 6):1013–1052. [PubMed: 9648540]

Mummery CJ, Ashburner J, Scott SK, Wise RJ. Functional neuroimaging of speech perception in six normal and two aphasic subjects. J Acoust Soc Am. 1999; 106:449–457. [PubMed: 10420635]

Musiek F, Mohanani A, Wierzbinski E, Kilgore G, Hunter J, Marotto J. Pathways: Will Wernicke’s area ever be defined? Hearing J. 2011; 64:6.

Neubert FX, Mars RB, Thomas AG, Sallet J, Rushworth MF. Comparison of human ventral frontal cortex areas for cognitive control and language with areas in monkey frontal cortex. Neuron. 2014; 81:700–713. [PubMed: 24485097]

Obleser J, Wise RJ, Alex Dresner M, Scott SK. Functional integration across brain regions improves speech perception under adverse listening conditions. J Neurosci. 2007; 27:2283–2289. [PubMed: 17329425]

Ojemann G, Ojemann J, Lettich E, Berger M. Cortical language localization in left, dominant hemisphere. J Neurosurg. 1989; 71:316–326. [PubMed: 2769383]

Ojemann GA. Brain organization for language from the perspective of electrical stimulation mapping. Behav Brain Sci. 1983; 6:189–206.

Ojemann GA. Cortical organization of language. J Neurosci. 1991; 11:2281–2287. [PubMed: 1869914]

Parker GJ, Luzzi S, Alexander DC, Wheeler-Kingshott CA, Ciccarelli O, Lambon Ralph MA. Lateralization of ventral and dorsal auditory-language pathways in the human brain. Neuroimage. 2005; 24:656–666. [PubMed: 15652301]

Passingham RE, Stephan KE, Kotter R. The anatomical basis of functional localization in the cortex. Nat Rev Neurosci. 2002; 3:606–616. [PubMed: 12154362]

Pataraia E, Billingsley-Marshall RL, Castillo EM, Breier JI, Simos PG, Sarkari S, Fitzgerald M, Clear T, Papanicolaou AC. Organization of receptive language-specific cortex before and after left temporal lobectomy. Neurology. 2005; 64:481–487. [PubMed: 15699379]

Price CJ. The anatomy of language: Contributions from functional neuroimaging. J Anat. 2000; 197(Pt 3):335–359. [PubMed: 11117622]

Price CJ, Crinion JT, Macsweeney M. A Generative Model of Speech Production in Broca's and Wernicke's Areas. Front Psychol. 2011; 2:237. [PubMed: 21954392]

Raichle ME, MacLeod AM, Snyder AZ, Powers WJ, Gusnard DA, Shulman GL. A default mode of brain function. Proc Natl Acad Sci USA. 2001; 98:676–682. [PubMed: 11209064]

Rauschecker JP, Scott SK. Maps and streams in the auditory cortex: Nonhuman primates illuminate human speech processing. Nat Neurosci. 2009a; 12:718–724. [PubMed: 19471271]

Rauschecker JP, Scott SK. Maps and streams in the auditory cortex: Nonhuman primates illuminate human speech processing. Nat Neurosci. 2009b; 12:718–724. [PubMed: 19471271]

Robinson JL, Laird AR, Glahn DC, Lovallo WR, Fox PT. Meta-analytic connectivity modeling: Delineating the functional connectivity of the human amygdala. Hum Brain Mapp. 2010; 31:173–184. [PubMed: 19603407]

Ross ED. Cerebral localization of functions and the neurology of language: Fact versus fiction or is it something else? Neuroscientist. 2010; 16:222–243. [PubMed: 20139334]

Sallet J, Mars RB, Noonan MP, Neubert FX, Jbabdi S, O'Reilly JX, Filippini N, Thomas AG, Rushworth MF. The organization of dorsal frontal cortex in humans and macaques. J Neurosci. 2013; 33:12255–12274. [PubMed: 23884933]

Sarubbo S, Le Bars E, Moritz-Gasser S, Duffau H. Complete recovery after surgical resection of left Wernicke's area in awake patient: A brain stimulation and functional MRI study. Neurosurgical Rev. 2012; 35:287–292.

Saur D, Kreher BW, Schnell S, Kummerer D, Kellmeyer P, Vry MS, Umarova R, Musso M, Glauche V, Abel S, Huber W, Rijntjes M, Hennig J, Weiller C. Ventral and dorsal pathways for language. Proc Natl Acad Sci USA. 2008; 105:18035–18040. [PubMed: 19004769]

Schleicher A, Amunts K, Geyer S, Morosan P, Zilles K. Observer-independent method for microstructural parcellation of cerebral cortex: A quantitative approach to cytoarchitectonics. Neuroimage. 1999; 9:165–177. [PubMed: 9918738]

Seghier ML. The angular gyrus: Multiple functions and multiple subdivisions. Neuroscientist. 2013; 19:43–61. [PubMed: 22547530]

Seghier ML, Fagan E, Price CJ. Functional subdivisions in the left angular gyrus where the semantic system meets and diverges from the default network. J Neurosci. 2010; 30:16809–16817. [PubMed: 21159952]

Shalom DB, Poeppel D. Functional anatomic models of language: Assembling the pieces. Neuroscientist. 2008; 14:119–127. [PubMed: 17911215]

Tanner DC. A redefining Wernicke's area: Receptive language and discourse semantics. J Allied Health. 2007; 36:63–66. [PubMed: 17633961]

Thiebaut de Schotten M, Urbanski M, Valabregue R, Bayle DJ, Volle E. Subdivision of the occipital lobes: An anatomical and functional MRI connectivity study. Cortex. 2014; 56:121–37. [PubMed: 23312799]

Tomasi D, Volkow ND. Resting functional connectivity of language networks: Characterization and reproducibility. Mol Psychiatry. 2012; 17:841–854. [PubMed: 22212597]

Turkeltaub PE, Eden GF, Jones KM, Zeffiro TA. Meta-analysis of the functional neuroanatomy of single-word reading: Method and validation. Neuroimage. 2002; 16:765–780. [PubMed: 12169260]

Wang J, Fan L, Zhang Y, Liu Y, Jiang D, Zhang Y, Yu C, Jiang T. Tractography-based parcellation of the human left inferior parietal lobule. Neuroimage. 2012; 63:641–652. [PubMed: 22846658]

Wang J, Yang Y, Fan L, Xu J, Li C, Liu Y, Fox PT, Eickhoff SB, Yu C, Jiang T. Convergent functional architecture of the superior parietal lobule unraveled with multimodal neuroimaging approaches. Hum Brain Mapp. 2015; 36:238–257. [PubMed: 25181023]

Wise RJ, Scott SK, Blank SC, Mummery CJ, Murphy K, Warburton EA. Separate neural subsystems within ‘Wernicke’s area’. Brain. 2001; 124:83–95. [PubMed: 11133789]

Zhang Y, Fan L, Zhang Y, Wang J, Zhu M, Zhang Y, Yu C, Jiang T. Connectivity-based parcellation of the human posteromedial cortex. Cereb Cortex. 2014; 24:719–727. [PubMed: 23146967]

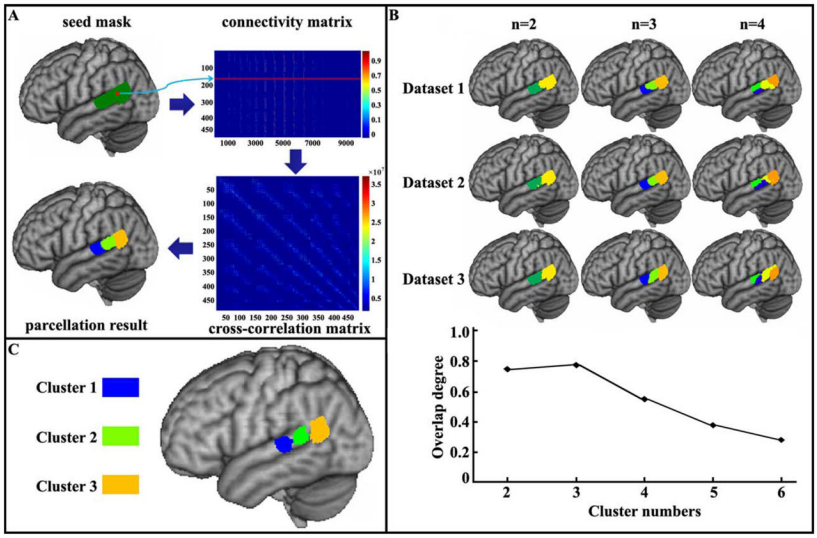

Figure 1.

Posterior superior temporal gyrus (STG) parcellation results yielded by tractography-based parcellation. (**A**) anatomical connectivity patterns-based parcellation was used to parcellate the Wernicke's area into component subregions. A liberal posterior STG mask including its adjacent area was first drawn on a structural MNI brain. Probabilistic tractography was performed from each voxel in the seed area and yielded a connectivity matrix between all voxels in the seed mask and each brain voxel. These connectivity matrices were then used to generate a symmetric cross-correlation matrix, which was then segmented for automated clustering to define different clusters/subregions. (**B**) for each number of clusters, the degree of overlap between the maximum probability maps yielded by tractography-based parcellation was calculated across the three datasets. C, the three-way parcellation of posterior STG was determined. To guide further analyses, the overlap of maximum probability maps across the three datasets was obtained. [Color figure can be viewed in the online issue, which is available at wileyonlinelibrary.com.]

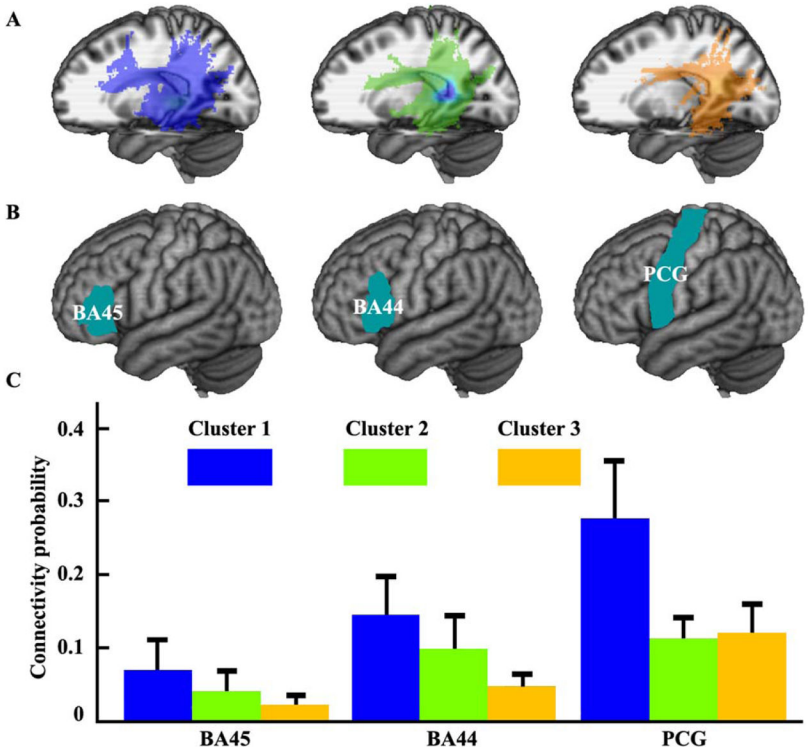

Figure 2.

Whole brain structural connectivity pattern and structural connection with specific targets for each subregion. (**A**) The whole brain population maps of the probabilistic tractography results of each subregion was portrayed. The main tract pathways include the superior longitudinal fasciculus (SLF) and arcuate fasciculus (AF). (**B**) The target masks including BA45, BA44, and precentral gyrus (PCG) were obtained by calculating the maximum probability map of each region using SPM Anatomy tool-box. (**C**) The mean anatomical connectivity probability and standard error of the mean for each subregion with each target brain area was calculated. [Color figure can be viewed in the online issue, which is available at wileyonlinelibrary.com.]

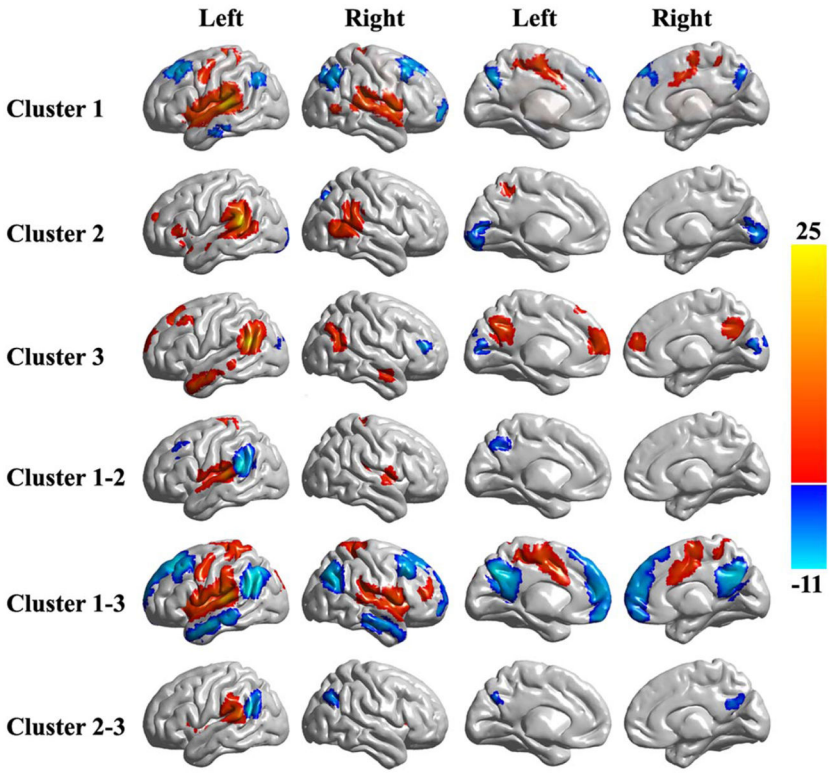

Figure 3.

Whole-brain RSFC pattern for each cluster and differences in the RSFC patterns between each pair of subregions. The RSFC patterns for each subregion was calculated and one-sample *t*-tests with correction for multiple comparisons were carried out by the family wise error (FWE) method with $P < 0.05$ and cluster size >30 voxels. Additionally, differences in the RSFC patterns between each pair of subregions were also obtained. And paired *t*-tests with corrections for multiple comparisons were carried out by the FWE method with $P < 0.05$ and cluster size >30 voxels. [Color figure can be viewed in the online issue, which is available at wileyonlinelibrary.com.]

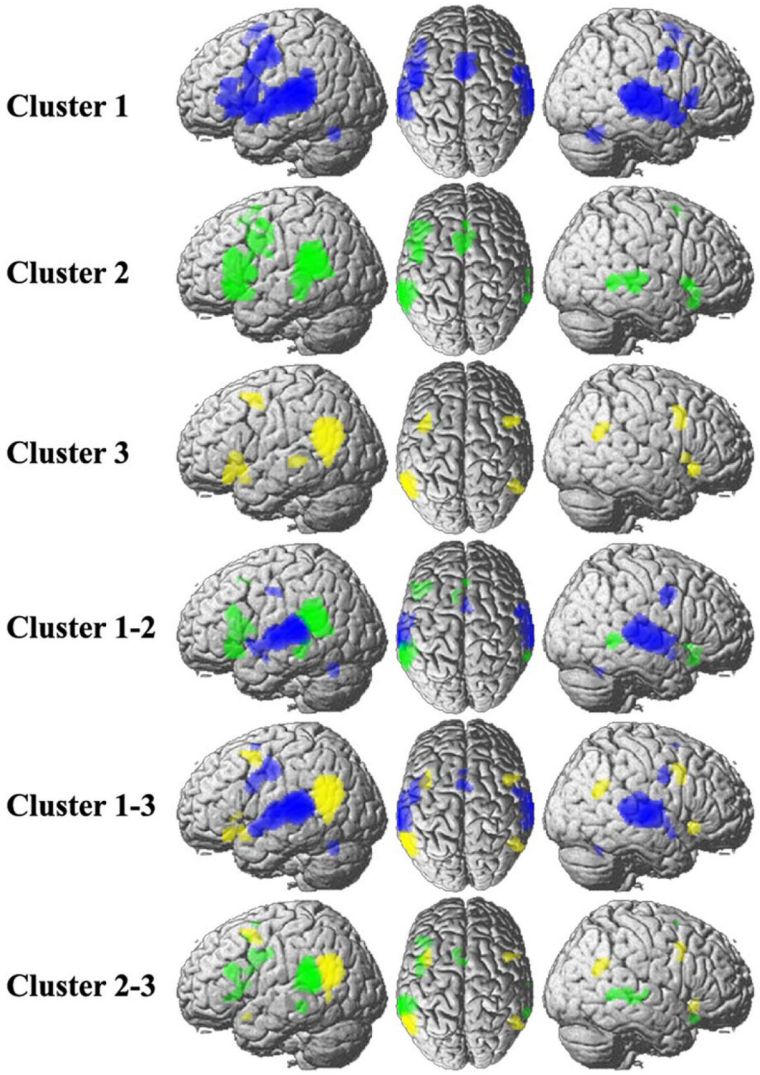

Figure 4.

The coactivation connectivity pattern for each subregion and contrast analyses. The whole brain coactivation connectivity pattern for each subregion was obtained using meta-analytical connectivity modeling (MACM) analyses (thresholded at $P < 0.05$, cluster-level FWE-corrected, cluster-forming threshold at voxel-level $P < 0.001$). To quantify the different coactivation connectivity pattern of each subregion, difference analysis on each pair of connectivity maps was performed to generate voxels that were significantly more likely coactivated with either subregion. [Color figure can be viewed in the online issue, which is available at wileyonlinelibrary.com.]

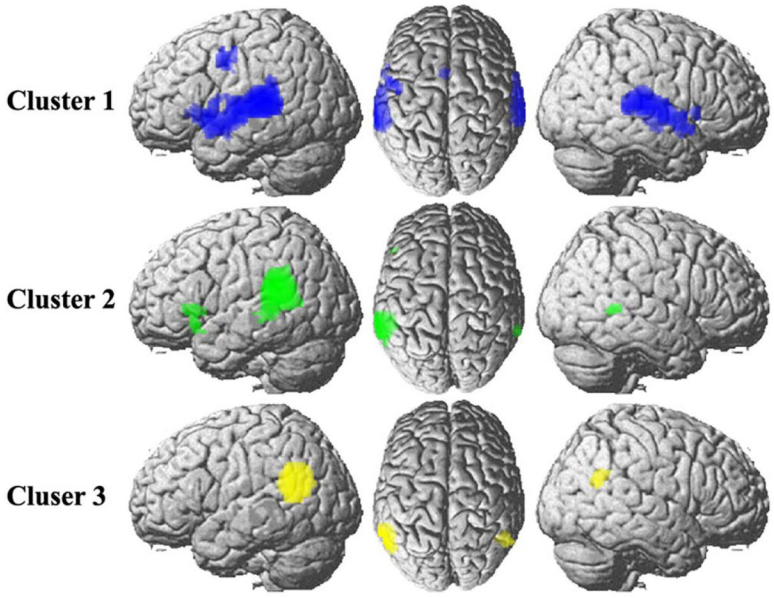

Figure 5.

Overlapping network shared by both resting-state network and task-dependent coactivation network. The overall network was calculated based on thresholded whole brain resting-state functional and coactivation connectivities by determining the intersection connectivity between the two modalities. [Color figure can be viewed in the online issue, which is available at wileyonlinelibrary.com.]

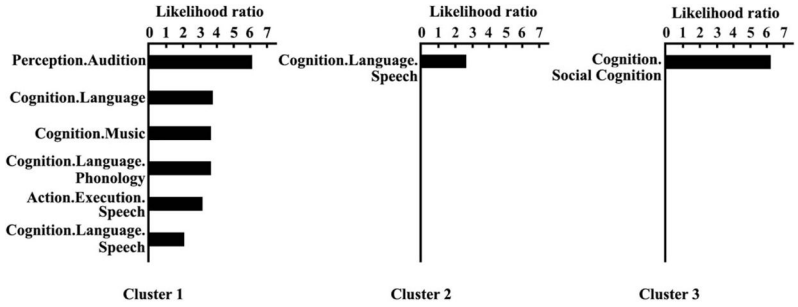

Figure 6.

Behavioral domains analyses of the left posterior STG subregions. Forward inference was used to determine the functional organization of each subregion. The significant activation probabilities for each subregion with respect to a given domain are depicted.

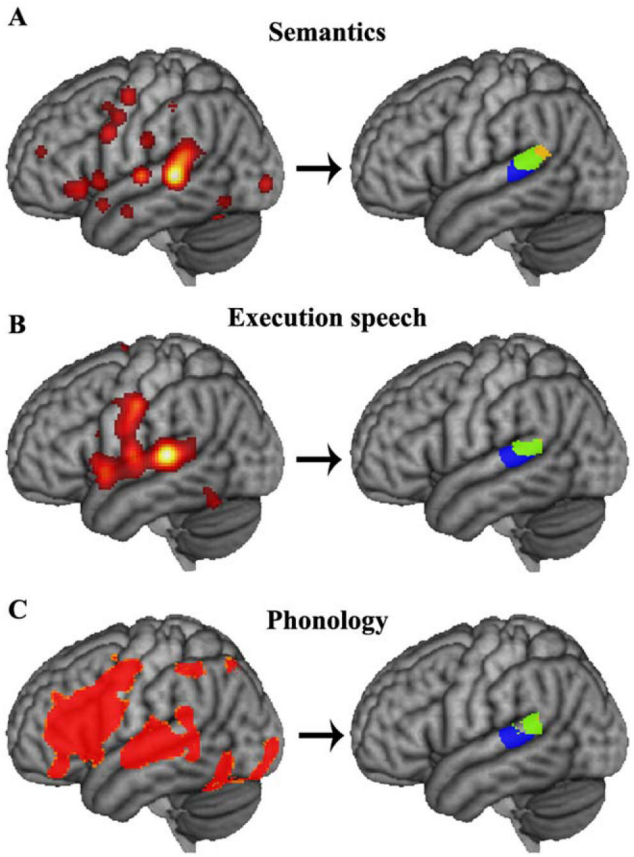

Figure 7.

Meta-analysis of semantics, execution speech and phonology to identify which subregion was mainly involved in language processing. (**A**) The semantics related network was identified by structure-based meta-analysis in defined "Wernicke's area". Then, the ALE maps were computed (false discovery rate (FDR) corrected: P <0.05 and minimum cluster dimension k >200 mm^3) and segmented into three clusters according to the parcellation results for Wernicke's area. (**B**) Execution speech related network was identified by calculating the ALE maps (FDR: P <0.05 and minimum cluster dimension k >200 mm^3), and the ALE map was also segmented into three clusters according to the parcellation results for Wernicke's area. (**C**) Phonology related network was identified using the same approach and segmented into three clusters according to the parcellation results for Wernicke's area. [Color figure can be viewed in the online issue, which is available at wileyonlinelibrary.com.]

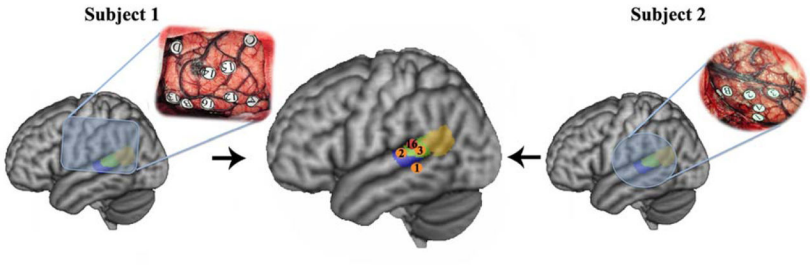

Figure 8.

Intraoperative electrical stimulation-positive results from two glioma patients in an object picture-naming task. The lateral surface views of the patients' brains in relation to the intraoperative electrical stimulation before tumor resection were shown in far left and right sides. The middle panel showed the positive-response sites during intraoperative electrical stimulation in the two patients. [Color figure can be viewed in the online issue, which is available at wileyonlinelibrary.com.]